Research & Reviews: A Journal of Physics
Volume 1, Issue 2, August 2012, Pages 9-18

STM JOURNALS

Study of Size Controllable Synthesis of Indium Tin Oxide Nanoparticles and Their Different Characterizations

A. Ayeshamariam[1], C. Sanjeeviraja[2]*
[1]Department of Physics, Khadir Mohideen College, Adirampattinam-614701, India
[2]School of Physics, Alagappa University, Karaikudi-630003, India

ABSTRACT

Nanocrystalline indium oxide powders were prepared by combustion synthesis. The changes of nanostructure caused by material processing were studied using X-ray powder diffraction (XRD), transmission electron microscopy (TEM), selected area electron diffraction (SAED) and Brummer Emette teller analysis (BET). The stoichiometric composition of the starting indium tin oxide powder (cubic in traces) induced phase transitions to high temperature. We found that the phase transition to ITO was initiated at the surface of the small particles, while transition from cubic to rutile started in their center. Changes in crystallite size during annealing process were obtained by the Scherer method, while the particle size changes were monitored by TEM. The difference in the results obtained by this combustion technique was explained in frame of basic physical properties characterizing both methods.

Keywords: *XRD, BET, TEM, FTIR.*

****Author for Correspondence*** E-mail: sanjeeviraja@rediffmail.com

1. INTRODUCTION

Quite recently, group II–VI semiconductor nanostructured materials were prepared by using a different method, as one of the well-established techniques for production of nanomaterial is combustion, compounds, oxides or composites. The recognition of common critical issues of control over nanostructure size and placement motivates sharing of solution over the boundaries of conventional disciplines is very essential. With precise control of the size of the particles, their characteristics can be adjusted in certain borders. But it is usually difficult to maintain these desired characteristics beyond different manufacturing processes to the final product. This is because loose nano-powders tend to grow to larger particles and/or firmly connected agglomerates already at room temperature and thus loosing their nano-specific characteristics. Transparent conducting oxide (TCO) nanoparticles of tin, indium and zinc oxides (doped and undoped) have been extensively studied due to their high optical transmittance and electrical conductivity. These particles are useful in photovoltaic and photo thermal applications [1–3] and the development and commercialization of transparent conducting oxides for electronic field as gas detectors, window heaters, solar cells, memory devices and flat panel display materials [4, 5]. If the particle size of a semiconductor becomes comparable to the Bohr radius, the ratio of surface atoms to those in the interior increases remarkably leading to the surface properties playing an important role in the properties of the material. The term “transparent conducting oxide (TCO)” refers to heavily doped oxide

semiconductors that have a band gap sufficiently large (≥ 3 eV) to make them transparent over the visible spectral range and a conductivity high enough such that they exhibit metal-like behavior. Due to their high conductivities, the powders also show high reflectivity in the near infrared. The synthesis and characterization of nanostructured n-TCOs is a very important and well-established field in nanotechnology and is still growing in stature. Therefore, the formation of nanocrystalline P-type counterpart may open up an extremely important and interesting field of research for the fabrication of all transparent nano-active devices. This will not only give a new dimension in the field of "Transparent Electronics" but new avenues may open up in the nanoparticles research keeping an eye on its tremendous applications in optoelectronics technology. Use of suitable raw material in combustion synthesis ensures stability of the chemical composition and high quality of products. More importantly, it should not react violently and should only produce nontoxic gases. Semi-conducting nanoparticles also exhibit a change in their electronic properties relative to that of the bulk counterpart as the size of the solid becomes smaller; the band gap becomes larger [6]. In addition, scientists have found that device characteristics in very small components are strongly altered by quantum mechanical effects. In many cases, these effects will undetermine the classical principles on which most of today's electronic components are based.

The chemical and physical properties of nanostructured materials depend on their geometry and hierarchical organization. The synthesis and characterization of nanostructured n-TCOs is a very important and well-established field in nanotechnology and is still growing in stature. This will not only give a new dimension in the field of "Transparent Electronics" but new avenues may open up in the nanoparticles research keeping an eye on its tremendous applications in optoelectronics technology.

If one considers integrating electronic, magnetic and photonic properties in the new generation devices should have high tunability of charge carriers, high carrier mobility, optical transparency, high abundance of the consisting elements and low impact on the environment. High conductivity of ITO is attributed to the high carrier concentration which is caused by incorporation of *Sn* ions into In_2O_3 host lattice and oxygen nonstochiometry. ITO has a cubic bixybite structure with the lattice parameter a = 10.118 A° [7]. Tin oxide is an n-type band semiconductor (E_g = 3.6 eV at 300 K), with interesting chemical, physical and mechanical properties, used in a variety of domestic, industrial, agricultural and medical applications, nanoelectronic devices, conductors, transistors, dye-based solar cells, transparent conducting electrodes, antistatic films, etc. The formation of doped tin oxide with different dopants using various methods has been used to improve optical properties

like luminescence, selectivity in gas mixtures, sensitivity and reducing degradation of performance with time and other properties.

Here, combustion process is applied to improve the particle size and uniformity of the problems. This process is to synthesize the ITO nanoparticle under heat treating circumstances reacting oxidation phased *In* and *Sn* with O_2, respectively. This synthesis has many advantages that the harmful nitric elements included in this synthesis are excluded. The heat-treating temperature can be lowered below 855 K, which is required to eliminate the harmful elements. Accordingly, highly pure and ultrafine particles can be achieved by applying this process. Use of suitable raw material in combustion synthesis ensures stability of the chemical composition and high quality of products. This work has been done with (NH_2 $CONH_2$) urea as fuel and Combustion heat (−2.98 kcal/g) [8].

2. EXPERIMENTAL PROCEDURE

2.1. Preparation of Precursor Materials

A calculated amount of $In(NO_3)_3$ (5.0 M), dissolved in minimum volume of water was added to the aqueous solution of $Sn(NO_3)_2$ obtained by stirring the *In*-metal ingots with concentrated HNO_3 for 40 h. The volume of $In(NO_3)_3$ solution and the weight of $Sn(NO_3)_2$ were taken by maintaining the *In/Sn* atomic ratio 90:10**.** The mixture was diluted with water and the resultant solution was stirred magnetically for 2 h. Urea was added to the above mixture till a gel of hydrated indium tin oxide appeared. It was stirred for additional 1 h at an ambient temperature. The pH of the above solution was maintained in the range 8.5–8.8 at this stage. The solution was stirred again for ½ h to ensure complete precipitation. The precipitation was placed in a hot plate at 100 °C for 20 min until it turned as gel. The resulting gel was then fired at a temperature higher than 350 °C until complete decomposition of the residues was achieved. The above procedure was repeated under different experimental conditions. The dried powders were calcined at different doping proportions to examine the crystallization behavior.

Here, different proportions of ITO particles were synthesized by the modified combustion of aqueous solutions containing stoichiometric amounts of the corresponding metal (Indium and tin) nitrates with fuel CH_2 (NO) CH_2 urea. The precursors have been introduced in such quantities insuring the right stoichiometry is obtained after combustion. We can calculate the numerical coefficients corresponding to a stoichiometric reaction from the total oxidizing and reducing valences of the reactants. Trivalent and divalent metals and the elements C, H, O have respectively valences of + 3, + 2, + 4, + 1 and −2; since during the combustion reaction, a conversion of nitrate in molecular nitrogen takes place, nitrogen is considered to have a valency of zero.

According to this analysis, the total oxidizing valency of $In(NO_3)_3{\cdot}3H_2O$ is (−15) and $Sn(NO_3)_2{\cdot}2H_2O$ is (−8) and Urea (+ 6). The molar number ψ can be calculated using the ratio of combustible/oxidant ratio. In order to obtain one mole of tin nitrate two moles of Indium nitrate ψ moles of fuel are then added.

In(−15) + Sn(−8) + ψ(+ 6) = 0

9(−15 + 1(−8) + (6) ψ = 0

Adiabatic flame temperature T_f of the combustion reaction is

$$T_f = 298 + \frac{\Sigma_{\text{Reactants}}(\gamma_i x\Delta H_{f,i}) - \Sigma_{products}(\gamma_j\ x\Delta H_{f,j})}{\Sigma_{proucts}\gamma_j xC_p} inK$$

ΔH_f = Enthalpy of formation of the products or the reactants respectively

C_p = Heat capacity of the products at constant pressure and at 298 K

γ = Molar number. The flame temperature was calculated as 855 K

This formula shows that the flame temperature not only depends on the nature of the fuel but also on the fuel to nitrate ratio (depending on the value of ψ).

When the reaction occurs, it is well known that the measured flame temperature is much lower than the calculated one because of non-adiabatic conditions (heat loss in ambient air) [9]:

ψ = 1, the reaction is stoichiometric (heat produced is maximum).

ψ < 1, the mixture is fuel lean (heat produced is less), in complete reaction.

ψ > 1, the mixture is fuel rich, combustion stops before reaction is completed.

On the other hand, Indium nitrate is utilized in the present study because of its dual role of being the Indium source and the Oxidant. Similar reaction equations for different metal nitrates and organic compounds can also be found in [10–13]. Note that $\psi = 1.0$ corresponds to the situation of "equivalent stoichiometric ratio," which complies that the oxygen content of Indium nitrate, tin nitrate can be completely reacted to oxidize/consume urea equivalently. As a result, ITO product and gases of CO_2, H_2O and N_2 can be formed directly from the reaction between fuel and outside.

The nano-powders were characterized by particle size analysis (Autosizer IIC Malvern) and powder X-ray diffraction (XRD) X-ray diffractometer (XRD) with monochromation CuK_α target (1.5406 A°) at a scan rate of 2 °/min. Unit cell parameter was calculated from the observed 'd'-spacing, which was accurately measured with the help of silicon as an internal standard. Particle size and morphology of the synthesized powders were further monitored with the help of a transmission electron microscope (TEM). The transmission electron micrograph was obtained on a JEOL JEM 200CX Transmission electron microscope. FITR studies of the ITO powders arrested during transformation to metal oxide were done in the range of 400–4000 cm^{-1} on a Nicolet 5pc FTIR Spectrometer.

3. RESULTS AND DISCUSSION

3.1. FTIR Spectra

Figure 1 indicates that the FTIR absorbance spectra of *In* and *Sn* based powders were fired at 350 ºC for 20 min. The spectra show characteristic vibrations in the region of 500 to 3500 cm^{-1}. The bands at 3285.18 and 3856.7 cm^{-1} are due to O–H species in the In- and Sn-based gel mixture which was heat treated at 105.51 ºC to 687.31 ºC, respectively and those at 1763.91 to 2359.71 cm^{-1} is due to C–H stretching frequencies. Notably, a broad band between 3285.18 cm^{-1} and 3856.7 cm^{-1} for all fired and heat treated samples was possible due to residual water present in the samples. The band seen in 1621.96 cm^{-1} is due to C = 0 arising due to bridging type Indium and tin metal bonding. The band at 1384.82 cm^{-1} is the C–O stretching frequencies and that at 1156.30 cm^{-1} is due to weakly bound nitric acid molecule (HOOC–N). The spectra of the samples, which were heat treated at 105.51 ºC to 687.31 ºC were nearly similar. Upon increasing heat treatment, temperature from 105.51 ºC to 687.31 ºC, the frequencies of O–H, C–H, C = O and In–ONOO–Sn bands decreased. The spectrum of ITO powder annealed at 601.98 ºC to 687.31 ºC, which shows an absence of absorption bands corresponding to organics and hydroxyls. The common features that appear below 827.42 cm^{-1} correspond to the stretching vibrations of *In = 0 and Sn = 0*, and also to the contributions of *In–0 and Sn–0* bonds. In the spectrum 601.98 ºC to 687.31 ºC, the band at 601.97 cm^{-1} may be assigned to the vibration of ITO powder bands that appear at high temperatures [14].

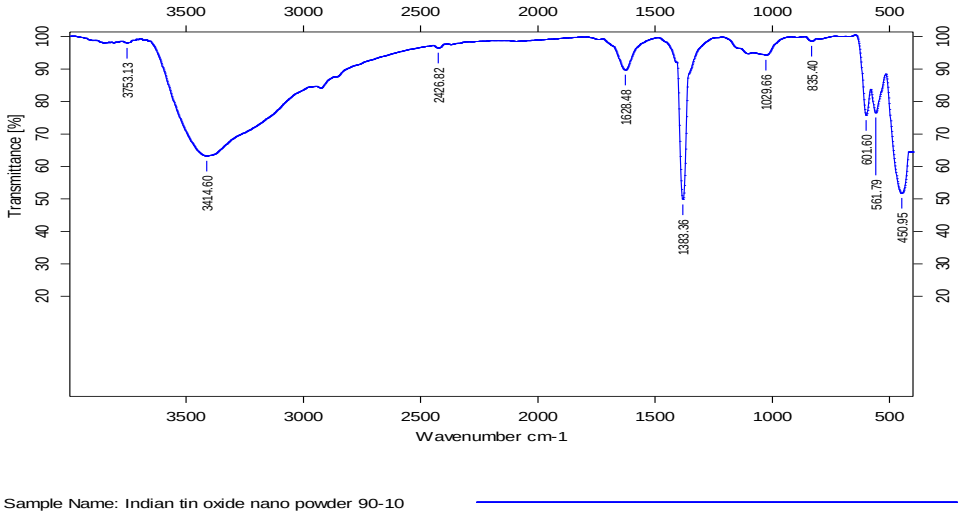

Fig.1: *FTIR Spectra of ITO (90:10).*

3.2. X-Ray Diffraction Studies

XRD measurements revealed that the ITO particles showed a cubic bixybite structure of indium tin oxide. The angles at which the peak intensities occur (Figure 2) are related to the inter-planar distances of the atomic structure

of In_2O_3 according to Bragg's law: $n\lambda = 2d\sin\theta$, where λ is the wavelength of X-ray radiation used, θ is the peak position angle and d is the inter-planar distance. The full width half maximum of each peak is the width (in degrees) at half the maximum peak intensity. The FWHM of a peak can be related to the average crystallite size. An estimate of the average crystallite size, of the particle is made by Debye Scherer equation and FWHM of the XRD peaks for different orientations. The more predominant orientations are 222, 400, 440 and 622 in the ITO crystal. These estimated values are compared with the standard values given for the lattice constants of ITO (89-4598). A characteristic shift towards lower angle compared to reflexes of ideal crystal is always observed for all peaks. This indicates a systematic lattice expansion. This phenomenon has also been reported by many other authors and some of them have been summarized. Particles in the peripheral position exhibit generally broader peaks, indicating larger micro-strain or smaller crystallite size and less pronounced 440 and 622 reflexes. All the peaks could be attributed to the ITO cubic phase and were indexed according to the JCPDS card number (89-4598) [15,16]. Therefore, the ITO films retain the bulk structure of ITO (a = 10.1309 A°) but exhibit a slight increase in the lattice constant (a = 10.22 A°) which was found to be in agreement with the literature. In this study, the lattice constant depends on the deposition of parameters and varies for ITO particles from 10.118 to 10.31 A°. In our work, the predominant peak exhibits a strong (222) orientation, revealed by the X-ray studies, indicating that these powders have a strong (222) texture, which is in good agreement with other structural observations reported in the literature [17]. XRD diffraction patterns of ITO powder of sample 1 (90:10) the peaks of 2θ equaling to 30.068, 34.729, 45.536, 50.630 and 59.745 and 20.93, 29.64, 34.73, 50.19, 60.18 and 76.07 are corresponding diffracted X rays of (211), (222), (400), (440), (622) and (444) planes respectively[18] (Table I).

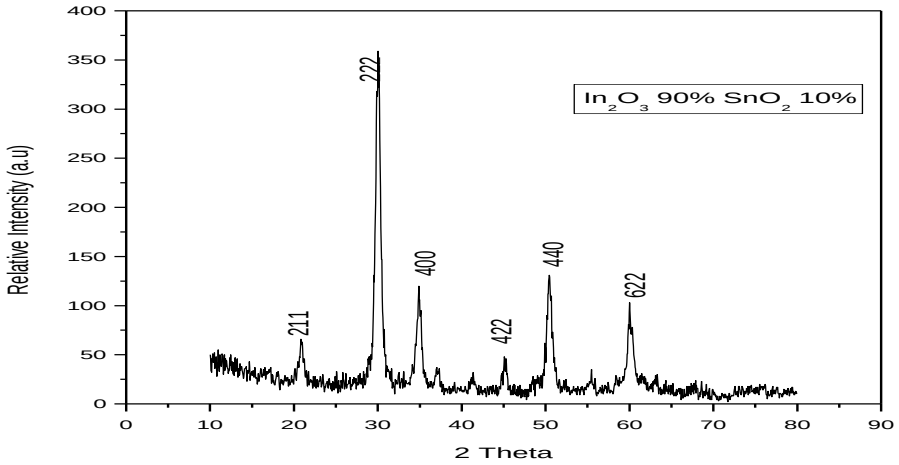

Fig. 2: *XRD Results of ITO (90:10).*

Table I: *XRD Structural Studies Result.*

Condition	Grain Size D (nm)	Dislocation Density x10^{18} lines/m^2	FWHM (β) Deg	Strain ε	Lattice Constant (A°)	Surface Area (m^2/g)
As prepared	8.776	0.01316	0.01723	0.00402	10.124	112
100 °C	11.049	0.0082	0.0136	0.0037	10.118	94
200 °C	11.142	0.0081	0.0135	0.00314	10.126	93
300 °C	12.174	0.0068	0.01233	0.00288	10.184	84
400 °C	13.043	0.00588	0.0115	0.00268	10.143	80
500 °C	17.217	0.000196	0.00872	0.00204	10.138	68

3.3. TEM

The morphology and microstructure of the product were further analyzed in TEM, which revealed that the product contains nanosized ITO particles. Figure 3 shows a TEM image, revealing the representative morphology of the ITO particles. The diameter of the ITO nanoparticles varies from 7 to 9 nm, averaged around 15 nm. The continuous regular arrays of the bright-dark contrasts (white arrow head) visible in the ITO nanoparticles in the magnified TEM image of Figure 4 are bend contours arising from dynamical electron diffraction effect from bending crystal, which shows that the nanoparticles are of monocrystalline nature. Selected-area electron microscopy (SAED) diffraction taken from one single ITO nanoparticles, shows complete diffraction pattern, indicating that the ITO nanoparticles are of single crystalline phase. It is confirmed that the crystal structure of ITO powder is cubic crystal structure [19] and the SnO_2 diffraction peak cannot be seen. The particle size from three cases are (XRD, BET, TEM) well matched with reported values of ITO nanoparticles also comparatively good agreement with one another.

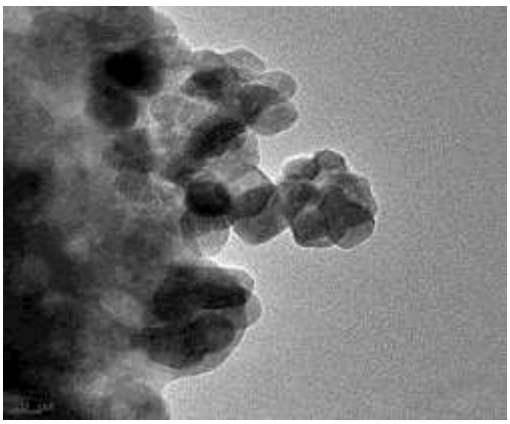

Fig. 3: *TEM Picture of ITO (90:10).*

Fig. 4: *SEAD Pattern of 90:10.*

3.4. BET Analysis

For Comparison, the XRD for indium tin oxide is estimated to be in the range between 10 and 12 nm [20]. From TEM observation we got for the as prepared sample as 9 nm. The particle size distribution of BET analysis confirmed the result as nearly equal to 12 nm. As the particle is annealed from 100 °C to 500 °C, the surface of the nanoparticle becomes rough. But, the rough surface becomes round again after heat treatment at 500 °C. Those phenomena are supposed to be based on the change in lattice structure by oxidation. That is, when heat-treated at 500 °C, surface roughness of the nanoparticle is slightly increased. However, as the heat-treating temperature is increased to 500 °C, the surface area is increased spontaneously in order to increase the surface energy. Therefore, the rough surface decreases the area as the heat-treating temperature is increased, and the surface area tends toward rounded shape of which area is reduced to the minimum. For more detailed investigation of particle size, BET-specific surface areas of the ITO nanoparticles were analyzed according to heat-treating temperature ranging from 100 °C to 500 °C. As a result, a considerable change according to the heat-treatment temperatures occurred as appeared in Figure 5. In case of heat treatment at 100, 200, 300, 400, and 500 °C, the surface areas of the ITO nanoparticles are 112, 94, 93, 84, 80, and 68 m^2/g, respectively. That is, sizes of the ITO nanoparticles are dependant upon heat treatment. The decreased specific surface area is attributed to agglomeration between the particle grains by diffusion. One of the mechanisms to decrease the nanoparticle size is owing to mainly grain boundary migration [21]. Therefore, the growth of nanoparticle can be suppressed as the heat-treating temperature is lowered. Therefore, it is confirmed that the ITO nanoparticle is more effective to synthesize a smaller-sized particle, and high quality using low (room) temperature (Table II).

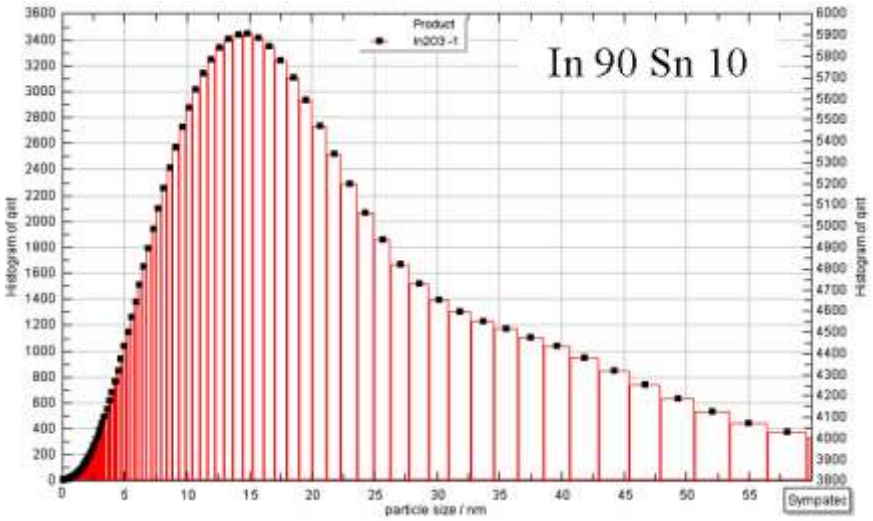

Fig. 5: *BET Analysis of 90:10.*

Table II: *Comparison of Particle Size.*

Sample (as prepared)	**XRD (nm)**	**TEM (nm)**	**BET (nm)**
ITO (90:10)	8.776	9	12.5

4. CONCLUSIONS

Proportion (10 atom%) tin-doped indium oxide powders with less than 15 nm in grain size which annealed in a furnace for 1 h at five different temperature ranges from 100 °C to 500 °C in air atmosphere were studied. The XRD results showed that the crystallinity of ITO powder was improved with annealing less than 20 nm in grain size obtained at different temperature which slowly increases with respect to temperature insteps of 100 °C. Particles are well grained in nature and their size decreases noticeably to a smaller value.

REFERENCES

1. Birkmire R. W., McCandless B. E., Hegedus S.S. et al. *International Journal of Solar Energy*. 1992. 12. 145p.
2. Ishibashi S., Higuchi Y., Ota Y., et al. *Journal of Vacuum Science and Technology*. 1990. A8. 1403p.
3. Kane J, Scweizer H. P. and Kern W. *Thin Solid Films*. 1975. 29. 155.
4. J. R. Bellingham, A. P. Mackenzie, W. A. Philips, et al. *Applied Physics Letters*, 1991. 58. 2506–2508p.
5. K. Osaza, T. Ye, Y. Aoyagi, et al. *Thin Solid Films*. 1994. 146. 58–64p.
6. Bender M., Seelig W., Daube C., et al. *Thin Solid Films*. 1998. 326. 72p.
7. D. Mergel, W. Stass, G. El, D. Barthel. *Journal of Applied Physics*. 2000. 88. 2437p.
8. Mukasyan A. S., Costllo C., Sherlock K. P., et al. *Separation and Purification Technology*. 2001. 25. 117p.
9. Manfacier J. C., Szepessy L., Bresse J. F., et al. *Materials Research Bulletin*. 1979. 14. 163p.
10. Bender M., Seelig W., Daube C., et al. *Thin Solid Films*. 1998. 326. 72p.
11. Djaoued Y., Phong V. H., Badilescu S, et al. *Thin Solid Films*. 1997. 293. 108. 682p.
12. D. Mergel, W. Stass, G. El, D. Barthel. *Journal of Applied Physics*. 2000. 88. 2437p.
13. Z. Qiao. PhD. Thesis, University of Duisburg – Essen, Gernany. 2003.
14. P. S. Devi, M. Chatterjee, D. Ganguli. *Materials Letters*. 2002. 55. 205p.
15. D. Mergel, W. Stass, G. El, D. Barthel. *Journal of Applied Physics*. 2000. 88. 2437p.
16. A. R. Stokes. *Proceedings of Physics Society*. 1948. 61. 382p.
17. Y. Meng, X. Yang, H. X. Chen, et al. *Thin Solid Films*. 2001. 394. 219p.

18. M. Buchanan, J. B. Webb, D. F. Williams. *Applied Physics Letters.* 1980. 37. 213p.
19. K. L. Chopra, S. Major, D. K. Pandya, et al. *Thin Solid Films*. 1983. 102. 1p.
20. K. Sreenivas, T. Sundarsena Rao, A. Mansnigh, et al. *Journal of Applied Physics*. 1985. 57(2). 384p.
21. Y. Meng, X. Yang, H. X. Chen, et al. *Thin Solid Films*. 2001. 394. 219p.
22. Hamberg, Granqvist, C. G. *Journal of Applied Physics*. 1986. 60. R123p.
23. Q. Pan, J. Xu, X. Dong, et al. *Sensors and Actuators B*. 2000. 66. 237p.

